



In vivo attachment site to attachment site length and strain of the ACL and its bundles during the full gait cycle measured by MRI and high-speed biplanar radiography

Zoë A. Englander^{a,b}, William E. Garrett^a, Charles E. Spritzer^c, Louis E. DeFrate^{a,b,d,*}

^a Department of Orthopaedic Surgery, Duke University, Durham, NC, USA

^b Department of Biomedical Engineering, Duke University, Durham, NC, USA

^c Department of Radiology, Duke University, Durham, NC, USA

^d Department of Mechanical Engineering and Materials Science, Duke University, Durham, NC, USA

ARTICLE INFO

Article history:

Accepted 17 October 2019

Keywords:

Flexion
Walking
Anterior cruciate ligament
Kinematics
Double bundle

ABSTRACT

The purpose of this study was to measure *in vivo* attachment site to attachment site lengths and strains of the anterior cruciate ligament (ACL) and its bundles throughout a full cycle of treadmill gait. To obtain these measurements, models of the femur, tibia, and associated ACL attachment sites were created from magnetic resonance (MR) images in 10 healthy subjects. ACL attachment sites were subdivided into anteromedial (AM) and posterolateral (PL) bundles. High-speed biplanar radiographs were obtained as subjects ambulated at 1 m/s. The bone models were registered to the radiographs, thereby reproducing the *in vivo* positions of the bones and ACL attachment sites throughout gait. The lengths of the ACL and both bundles were estimated as straight line distances between attachment sites for each knee position. Increased attachment to attachment ACL length and strain were observed during midstance (length = 28.5 ± 2.6 mm, strain = $5 \pm 4\%$, mean \pm standard deviation), and heel strike (length = 30.5 ± 3.0 mm, strain = $12 \pm 5\%$) when the knee was positioned at low flexion angles. Significant inverse correlations were observed between mean attachment to attachment ACL lengths and flexion ($\rho = -0.87$, $p < 0.001$), as well as both bundle lengths and flexion ($\rho = -0.86$, $p < 0.001$ and $\rho = -0.82$, $p < 0.001$, respectively). AM and PL bundle attachment to attachment lengths were highly correlated throughout treadmill gait ($\rho = 0.90$, $p < 0.001$). These data can provide valuable information to inform design criteria for ACL grafts used in reconstructive surgery, and may be useful in the design of rehabilitation and injury prevention protocols.

© 2019 Elsevier Ltd. All rights reserved.

1. Introduction

There is presently very limited *in vivo* data to describe how the anterior cruciate ligament (ACL) functions throughout the gait cycle, which is a common activity of daily living (Taylor et al., 2013; Wu et al., 2010). Improved understanding of how the ACL functions to stabilize the knee joint during gait may help to inform design criteria for grafts used in ACL reconstruction (Beynon and Fleming, 1998). Furthermore, such information may be useful in the design of rehabilitation (Fleming et al., 2001; Heijne et al., 2004) and injury prevention protocols (Shin et al., 2011), as well as in the validation of mathematical models of ACL function (Shelburne et al., 2004; Weinhandl et al., 2016).

To investigate ACL function *in vivo*, three-dimensional (3D) models of the femur, tibia, and associated ACL attachment sites, derived from magnetic resonance (MR) images, can be registered to biplanar radiographs in order to reproduce the positions of the bones at the time of radiographic imaging (Englander et al., 2018, 2019; Li et al., 2004; Taylor et al., 2011, 2013; Utturkar et al., 2013). ACL lengths are then estimated for each knee position by measuring the distances between the centers of the tibial and femoral attachment sites (Li et al., 2005). Furthermore, the attachment to attachment lengths of the anteromedial (AM) and posterolateral (PL) bundles of the ACL can be investigated similarly by subdividing the attachment sites (Englander et al., 2019; Jordan et al., 2007; Li et al., 2004; Petersen and Zantop, 2007; Utturkar et al., 2013).

These techniques have been used in several studies to estimate *in vivo* ACL lengths for static or quasi-static knee postures (Li et al.,

* Corresponding author at: Room 379, Medical Sciences Research Bldg, Box 3093, Duke University Medical Center, Durham, NC 27710, USA.

E-mail address: lou.defrate@duke.edu (L.E. DeFrate).

2004; Utturkar et al., 2013) and during the stance phase of gait (Wu et al., 2010). ACL lengths during dynamic activities have been estimated by integrating 3D models and static biplanar radiographs with kinematic data obtained using optical marker-based motion capture (Taylor et al., 2013; Taylor et al., 2011). More recently, a technique has been developed to achieve automatic registration of MR-based bone models to high-speed biplanar radiographs (Englander et al., 2018, 2019). This technique (Englander et al., 2018) is particularly advantageous in measuring dynamic changes in ACL length with high precision in that it removes the potential for error that may be introduced by the movement of markers on the skin relative to the underlying bone (Taylor et al., 2013) while maintaining a high temporal resolution.

The present study builds on these principles to measure the attachment site to attachment site lengths of the ACL and its AM and PL bundles during an entire cycle of treadmill gait. Based on prior literature (Taylor et al., 2013), we hypothesized that attachment site to attachment site ACL length and strain (defined as the changes in ACL length normalized to its length at the time of MR imaging) would be influenced by knee flexion angle throughout the gait cycle. We also hypothesized that AM and PL bundle attachment site to attachment site lengths would show a similar relationship to flexion angle as the overall ACL length (Wu et al., 2010).

2. Materials and methods

Ten healthy subjects (3 female and 7 male, body mass index (BMI): 24.3 ± 2.0 kg/m², age: 28.6 ± 3.4 years, mean \pm standard deviation) with no previous history of lower extremity injury or surgery prior to testing were evaluated using an IRB approved protocol. All subjects provided written informed consent. The right knee of each subject was imaged using a 3T magnetic resonance imaging (MRI) scanner (Trio Tim, Siemens Medical Solutions USA). Sagittal, coronal, and axial images were acquired from the subjects while lying supine, using a high resolution double-echo steady-state sequence (DESS) and an eight-channel knee coil (resolution: $0.3 \times 0.3 \times 1$ mm; flip angle: 25° , repetition time: 17 ms, echo time: 6 ms). Outlines of the femur and tibia, as well as the outer margins of the ACL attachment sites on the femur and tibia were segmented manually using solid-modeling software in all three planes (Rhinoceros 4.0, Robert McNeel and Associates) (Fig. 1). These outlines were compiled into 3D models of the joint (Geomagic Studio, 3D Systems) (Abebe et al., 2009; Collins et al., 2018; Kim et al., 2015; Li et al., 2005; Owusu-Akyaw et al., 2018). The positions and shapes of the ligament attachment sites were confirmed in the three orthogonal imaging planes. Prior validation studies have demonstrated that this approach can locate the center of the ACL footprint with an accuracy of 0.3 ± 0.2 mm (mean \pm standard deviation) (Abebe et al., 2009; Taylor et al., 2013).

Additionally, the attachment sites of the ACL on the femur and tibia were divided into anteromedial (AM) and posterolateral (PL) bundles as described previously (Jordan et al., 2007; Utturkar et al., 2013) (Fig. 2). Specifically, we estimated the AM and PL bundle subdivisions by dividing the overall ACL attachment site footprints such that half of the footprint surface area was contained in the anterior and medial aspect of the attachment site and half was contained within the posterior and lateral aspect of the attachment site.

Following the MR image acquisition, the subjects were imaged using a high-speed biplanar radiography system consisting of two x-ray generators (EMD technologies), two x-ray tubes (G296, Varian), and two image intensifiers (41 cm diameter, TH 9447 QX, Thales), which were coupled to two high-speed cameras

(Phantom v9.1, Vision Research). Each radiograph had a matrix size of 1152×1152 pixels². First, the positions of the sources and intensifiers were adjusted in order to ensure that the full gait cycle could be captured within the field-of-view without interference from the contralateral leg. Next, calibration images were acquired in order to map the geometry of the biplanar radiography system set up, as described previously (Englander et al., 2018). A calibration plate consisting of 4500 regularly spaced stainless steel beads was imaged on each intensifier. These images were used to correct for the inherent distortion in the radiographs (Reimann and Flynn, 1992) in post-processing, as previously described (Englander et al., 2018).

Subjects ambulated at a speed of 1 m/s on an instrumented dual belt treadmill (Bertec) that was used to record the ground reaction force at a sampling rate of 1200 Hz. High-speed biplanar radiographs were obtained at a frame rate of 120 Hz as the subject walked. Approximately two seconds of radiographic data were collected for each trial. The data was then visually inspected. The trial was considered valid unless either the tibia or femur extended completely outside of the field-of-view of the imaging system (Englander et al., 2018). A second trial was recorded only if needed, in order to minimize radiation exposure to the participant. Each study used a radiographic protocol not exceeding 110 kVp/200 mA. The pulse width of each exposure was 1.5 ms. The radiation effective dose (a weighted average of absorbed doses to bone surfaces, skin and soft tissues) was calculated by Duke Radiation Safety from the total skin entrance exposure and energy absorption by the tissues to assess radiation risk to subjects. The total effective dose was found to be less than 0.14 mSv per participant, which is comparable to the effective dose from fluoroscopy-guided clinical hip procedures (about 0.3 mSv) and is considerably less than the annual natural background radiation in the US (2.4–3.1 mSv) (Budd et al., 2012; Mettler Jr et al., 2009; NCRP, 2010).

Following data collection, the 3D bone models, the calibration images, and biplanar radiographs were imported into custom registration software (Englander et al., 2018). Subsequently, the software was employed to move each bone separately within 6 degrees of freedom until its projections onto the two imaging planes from the perspective of the radiographic sources matched the outlines of bones as seen in the radiographs (Fig. 3). Previous validation of this technique has been shown to have a precision of approximately 70 μ m in measuring the relative distances between two matched bones (Englander et al., 2018).

After reproducing the *in vivo* positions of the bones during the full gait cycle (Fig. 4), the attachment site to attachment site lengths of the ACL and its bundles, as well as knee flexion angles, were measured from the 3D models of the joint (Englander et al., 2019; Utturkar et al., 2013). Flexion angle was defined as the angle between the long axes of the femur and tibia about the femoral transepicondylar axis. ACL length was defined as the distance between the centers of the femoral and tibial attachment sites (Li et al., 2005). Similarly, the lengths of the AM and PL bundles were defined as the distances between the centers of their attachment sites subdivisions. Since it is difficult to measure the slack-taut transition of a ligament in living subjects (Fleming and Beynon, 2004), attachment site to attachment site ACL strain was defined at local maxima as the change in ACL length normalized to its length in a non-weight bearing state during MR imaging (Taylor et al., 2011).

Heel strikes were determined from the vertical component of the ground reaction force. Specifically, the heel strikes (designated as 0 and 100% of gait) were defined as the first data point where force registered on the force plate after the swing phase of gait. All measurements were interpolated from the data to represent values of each variable as a function of % gait cycle in 2% increments. This normalization procedure was performed in order to

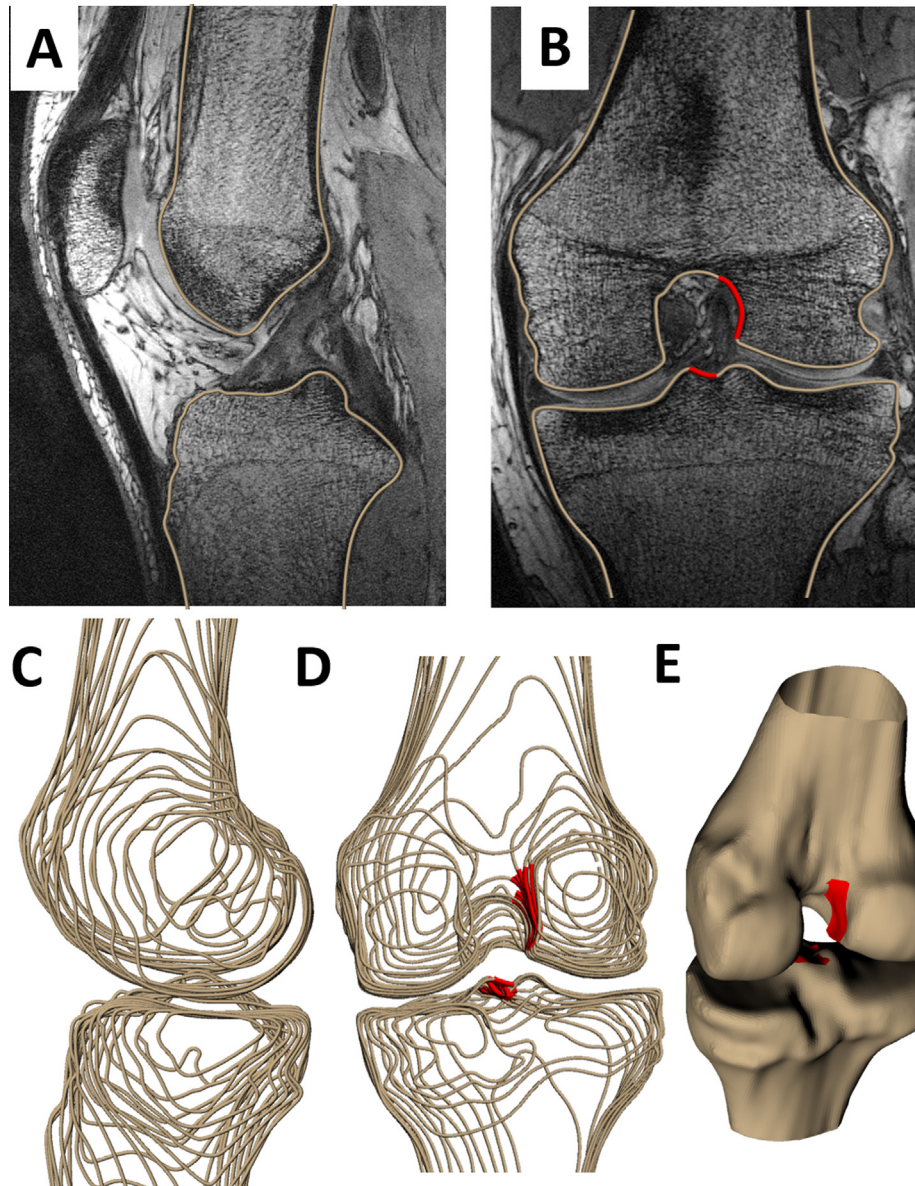


Fig. 1. The outer contours of the femur and tibia were outlined in double echo steady state (DESS) magnetic resonance (MR) images in the (A) sagittal plane (B) coronal plane and axial plane (not shown). (B) ACL attachment sites were outlined in the coronal plane (shown in red). These contours were compiled into wireframe models (C, D) and converted into 3D surface models of the femur and tibia and associated ACL attachment sites. (E) The coronal model was registered to the sagittal model to generate a surface model with an appropriately positioned ACL attachment site (shown in red). ACL attachment site locations were confirmed in all three planes. (For interpretation of the references to colour in this figure legend, the reader is referred to the web version of this article.) Figured adapted from Englander et al., 2019a.

allow for the comparison of data across subjects (Englander et al., 2018).

Data analyses were performed using Matlab (version R2016B, Mathworks). Alpha was set at 0.05 for all statistical tests. A Spearman-rho rank correlation was performed to test for a relationship between mean (across subjects at each percent gait cycle) attachment site to attachment site ACL length and mean flexion angle throughout the gait cycle. Furthermore, the relationships between mean AM and PL bundle attachment site to attachment site lengths and mean flexion angle, as well as mean AM and mean PL bundle lengths were quantified similarly.

In a subset of 3 subjects, a sensitivity analysis was performed to assess the influence of variations in the locations of the centers of the attachment sites on the patterns of attachment site to attachment site ACL length. Specifically, in each of the 3 subjects, the locations of the femoral and tibial attachment site centers were varied 20 times within a 5 mm radius of the original attachment

site centers, and the distances between these points were measured throughout gait. Spearman-rho correlations were used to assess the relationships throughout gait between the length measured from the varied attachment site centers and the length measured from the original ACL attachment site centers. A similar sensitivity analysis was performed for both the AM and PL bundle attachment site centers. Spearman-rho correlations were again used to assess the relationships between distances measured between the varied AM and PL attachment site centers and distances measured between the original AM and PL attachment site centers throughout gait.

3. Results

The average attachment site to attachment site length of the ACL measured at the time of MR imaging was 27.3 ± 3.5 mm

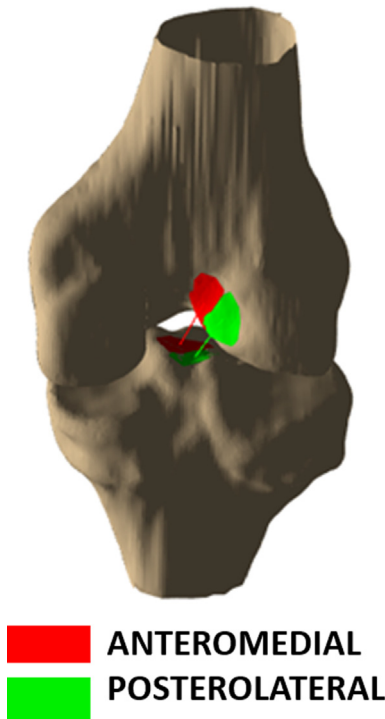


Fig. 2. Example of estimated subdivisions of the ACL attachment sites into its anteromedial and posterolateral bundles.

(mean ± standard deviation). The average knee flexion angle at the time of MR imaging was $8 \pm 2^\circ$. The average attachment site to attachment site lengths of the AM and PL bundles at the time of MR imaging were 29.4 ± 3.8 mm and 25.0 ± 2.1 mm, respectively. The means and standard deviations of flexion angle and attachment site to attachment site ACL length as a function of the

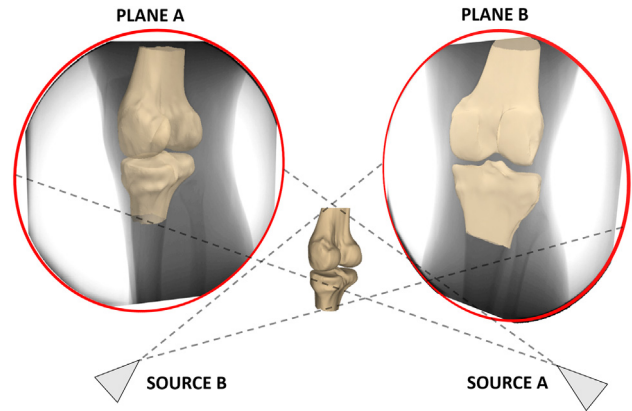


Fig. 3. Each bone was moved separately within 6 degrees of freedom until its projections onto the two imaging planes from the perspective of the radiographic sources matched the bones as seen in the radiographs. Previous validation of this technique has demonstrated a precision of approximately $70 \mu\text{m}$ in measuring the relative distances between two matched bones.

percentage of the gait cycle are plotted in Fig. 5. Local maxima in attachment site to attachment site ACL length and strain were observed during midstance (length = 28.5 ± 2.6 mm, strain = $5 \pm 4\%$, mean ± standard deviation) and heel strike (length = 30.5 ± 3.0 mm, strain = $12 \pm 5\%$) when the knee was positioned at low flexion angles ($-2 \pm 8^\circ$ and $-4 \pm 10^\circ$, respectively).

Furthermore, a significant inverse relationship between attachment site to attachment site ACL length and flexion angle ($\rho = -0.87$, $p < 0.001$) was observed, such that the mean attachment site to attachment site ACL length generally increased with knee extension throughout gait (Fig. 6). Similarly, both AM and PL bundle attachment site to attachment site lengths were significantly inversely correlated with flexion angle ($\rho = -0.86$, $p < 0.001$ and $\rho = -0.82$, $p < 0.001$) (Fig. 6). AM and PL bundle

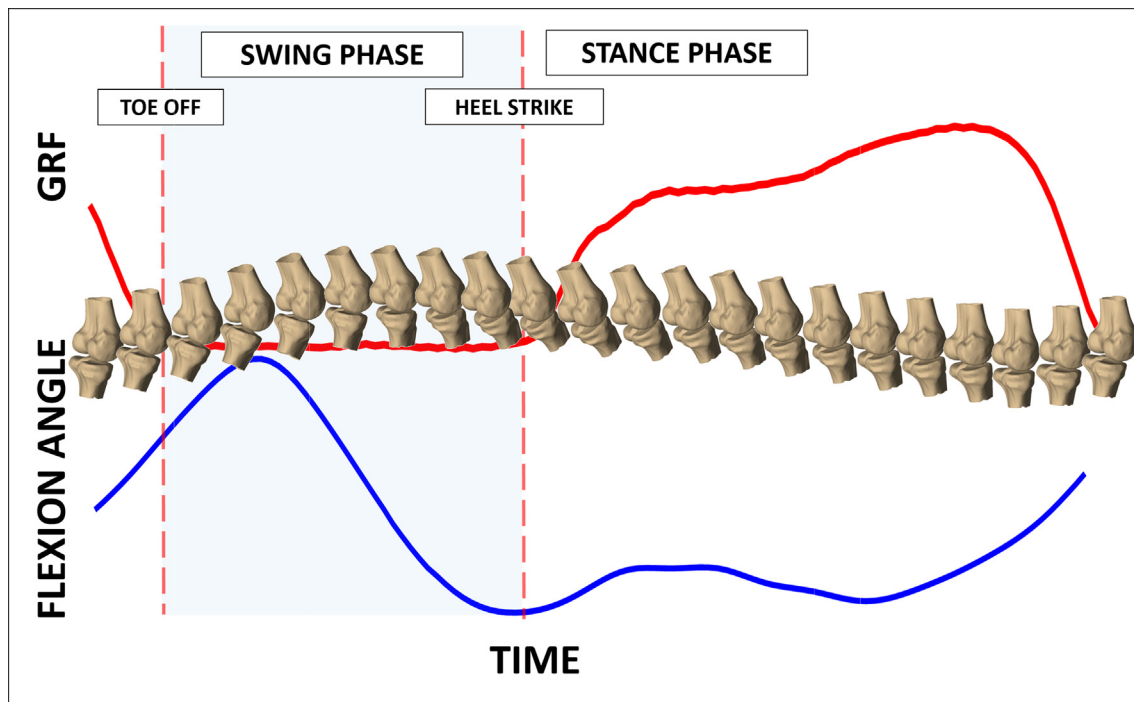


Fig. 4. The *in vivo* positions of the bones were reproduced during the gait cycle (example of a single subject). Using the ground reaction forces (GRF), heel strike (designed as 0 and 100% of the gait cycle) was identified and the data was normalized to between 0 and 100% of the gait cycle in increments of 2% to enable comparison across subjects.

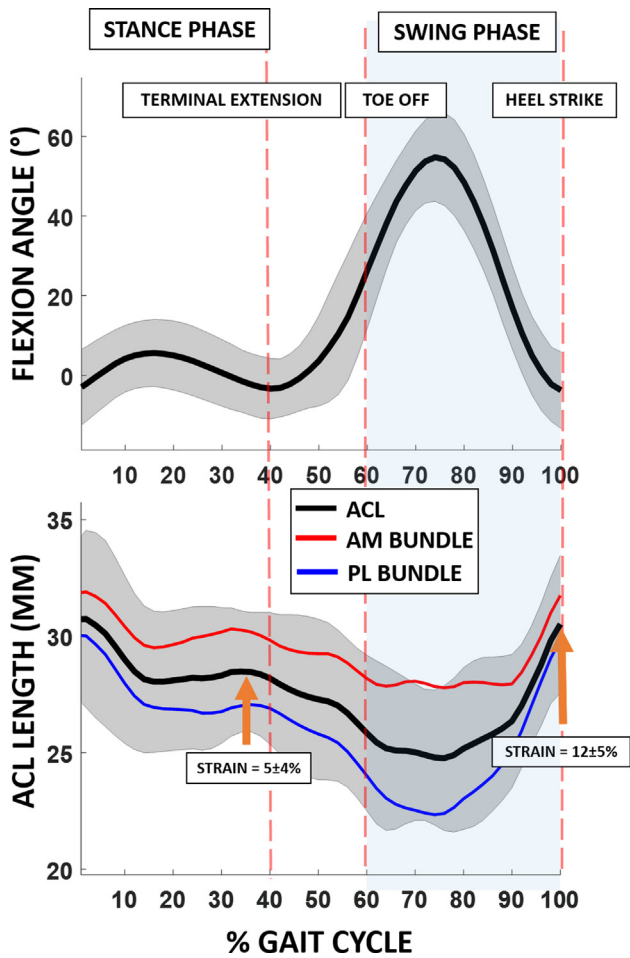


Fig. 5. Flexion angle and attachment site to attachment site ACL length are shown as a function of % gait cycle. Local maxima in attachment site to attachment site ACL length and strain were observed during midstance (length = 28.5 ± 2.6 mm, strain = $5 \pm 4\%$, mean \pm standard deviation), and during heel strike (length = 30.5 ± 3.0 mm, strain = $12 \pm 5\%$) when the knee was positioned at low flexion angles ($-2 \pm 8^\circ$ and $-4 \pm 10^\circ$, respectively). Attachment site to attachment site ACL strain is defined as the change in length of the ACL in each knee position during gait, normalized to the length of the ACL in its minimally loaded state during MR imaging.

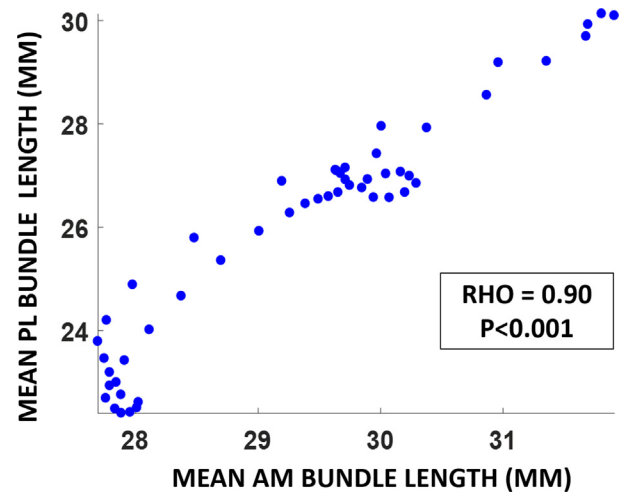


Fig. 7. AM and PL bundle attachment site to attachment site lengths were highly correlated with each other throughout gait ($\rho = 0.90$, $p < 0.001$).

lengths were highly correlated with each other ($\rho = 0.90$, $p < 0.001$) (Fig. 7).

In the sensitivity analysis, we found that the patterns of attachment site to attachment site ACL and bundle lengths during gait were robust to changes in the locations of the attachment sites. Specifically, the mean Spearman-rho rank correlation coefficient across subjects reflecting the relationship between the original ACL length and the varied attachment site ACL lengths was $\rho = 0.98 \pm 0.01$ (mean \pm standard deviation across subjects). Furthermore, the relationship between the original AM and PL bundle lengths and the varied attachment site lengths were $\rho = 0.88 \pm 0.06$ and $\rho = 0.90 \pm 0.06$. All of these correlations were statistically significant with $p < 0.05$.

4. Discussion

The present study integrated 3D models of the knee joint created from MR images with high-speed biplanar radiographs (Englander et al., 2018, 2019) to measure *in vivo* attachment site to attachment site ACL lengths and strains during a full cycle of treadmill gait. Local maxima in attachment site to attachment site

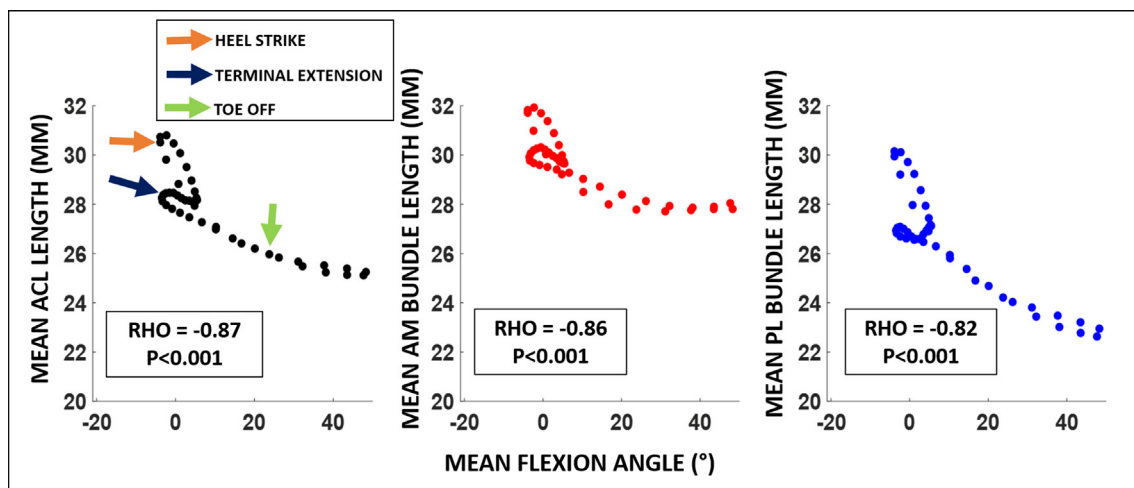


Fig. 6. Spearman's rho correlation demonstrated a significant inverse correlation between attachment site to attachment site ACL length and flexion angle ($\rho = -0.87$, $p < 0.001$), such that mean attachment site to attachment site ACL length generally decreased with increasing mean knee flexion throughout gait. Furthermore, both AM and PL bundles attachment site to attachment site lengths were significantly inversely correlated with flexion angle ($\rho = -0.86$, $p < 0.001$ and $\rho = -0.82$, $p < 0.001$).

ACL length and strain were observed during midstance and at heel strike, when the knee was positioned near extension. Furthermore, this study identified a statistically significant inverse relationship between knee flexion angle and attachment site to attachment site ACL length, such that length generally increased with knee extension (Fig. 6). This relationship held for the overall attachment site to attachment site ACL lengths, as well as the attachment site to attachment site AM and PL bundle lengths. Furthermore, AM and PL bundle lengths were highly correlated with each other throughout gait (Fig. 7). This study is significant in that here we report *in vivo* attachment site to attachment site lengths of the ACL and its bundles throughout an entire cycle of treadmill gait.

The findings of this study are in line with the present literature regarding *in vivo* ACL function during gait (Englander et al., 2018; Taylor et al., 2013; Wu et al., 2010). Specifically, Wu et al. (2010) measured ACL length during the stance phase and also demonstrated peaks in both AM and PL bundle lengths associated with midstance and heel strike, similar to the data presented here. Additionally, Taylor et al. (2013) utilized marker-based motion capture, MR imaging, and static biplanar radiography to measure ACL length throughout the gait cycle. Also in consilience with the present study, this study identified two peaks in attachment site to attachment site ACL length, the first during midstance and the second associated with heel strike. Importantly, the studies by Wu et al. (2010) and Taylor et al. (2013) were further in agreement with the data presented here in that they identified a strong inverse correlation between knee flexion angle and ACL length, with peaks in ACL length and strain occurring when the knee was positioned in low flexion angles. Additionally, the present study complements this prior literature in that the direct registration of the bone models to high-speed biplanar radiographs eliminates potential for error associated with the kinematic markers moving relative to the underlying bone that may occur using motion capture techniques (Taylor et al., 2013). Furthermore, this study provides estimates of attachment site to attachment site ACL length throughout the gait cycle at a high temporal resolution.

The finding that attachment site to attachment site ACL length is inversely related to knee flexion angle is in agreement with previous *in vivo* studies that have used arthroscopically implanted strain gauges (Beynon and Fleming, 1998; Cerulli et al., 2003; Fleming et al., 2001) and imaging techniques (Englander et al., 2019c; Taylor et al., 2013; Taylor et al., 2011; Utturkar et al., 2013) to show that ACL length increases with knee extension for various knee postures or motions. While joint loading during gait involves complex dynamic three dimensional loading conditions, including joint compression (Marouane et al., 2014; Marouane et al., 2015; Meyer and Haut, 2005, 2008; Shelburne et al., 2004; Torzilli et al., 1994), a potential mechanism of ACL loading with knee extension involves quadriceps activation. Specifically, *in vivo* imaging studies have indicated that the patellar tendon is oriented such that quadriceps activation generates an anteriorly directed shear force on the tibia when the knee is positioned at a low flexion angle (DeFrate et al., 2007; Englander et al., 2019c; Nunley et al., 2003). As a primary function of the ACL is to resist anterior tibial translation (Butler et al., 1980), increased quadriceps activation acting via the patellar tendon when the knee is extended may result in increased anterior tibial shear and loading of the ACL. In line with this hypothesis, a number of cadaver studies have demonstrated increased ACL strain with simulated quadriceps contraction (Arms et al., 1984; Berns et al., 1992; Dürselen et al., 1995; Markolf et al., 1990), in particular with the knee positioned at a low flexion angle (DeMorat et al., 2004; Draganich and Vahey, 1990; Mesfar and Shirazi-Adl, 2005). This hypothesis is also in agreement with *in vivo* studies that have directly measured ACL strain during isometric quadriceps contraction using strain transducers (Beynon and Fleming, 1998). Furthermore, with regard to the

increased attachment site to attachment site ACL length observed during heel strike and midstance, electromyography studies have indicated that the quadriceps fire prior to heel strike and continue to be activated at the beginning of the stance phase during weight acceptance (Huber et al., 2011; Shelburne et al., 2004).

In this study, the overall attachment site to attachment site length of the ACL and its bundles are each represented by the straight line distance between attachment site footprints. However, the ACL is a complex structure comprised of many fibers, (Arnoczky, 1983; Hara et al., 2009; Nawabi et al., 2016; Odensten and Gillquist, 1985; Petersen and Zantop, 2007; Skelley et al., 2017) and thus these straight line distance measurements represent approximations of ACL length. Importantly, studies have noted that selection of the ACL attachment sites may affect the estimates of ligament length during the flexion path (Hefzy and Grood, 1986; Li et al., 2004). To address this concern, we performed a sensitivity analysis to assess the dependence of the attachment site to attachment site ACL length measurements on the locations of the attachment sites. The strong correlations observed in these analyses suggest that variability in the locations of the attachment sites would not affect our overall conclusions regarding attachment site to attachment site ACL length patterns during gait. This sensitivity analysis is in agreement with a similar analysis performed by Li et al. (2004), which determined that a 5 mm variation in the location of the attachment site footprints had minimal effect on the observed relationship between ACL length and flexion angle during a quasi-static lunge. Thus, these results suggest that strains and lengths may be maximized during the same portions of the gait cycle even with variability in how the attachment sites are defined.

With regard to ACL bundle function, some cadaver studies have suggested that the AM and PL bundles of the ACL behave reciprocally, with the posterolateral (PL) bundle being taut at low flexion angles and the anteromedial (AM) bundle being taut at high flexion angles (Gabriel et al., 2004; Girgis et al., 1975; Petersen and Zantop, 2007). However, there remains discrepancy in the literature regarding the subdivisions of the ACL (Petersen and Zantop, 2007; Skelley et al., 2017). Specifically, some cadaveric dissections have identified two or more distinct bundles (Amis and Dawkins, 1991; Norwood JR and Cross, 1977; Otsubo et al., 2012), while other studies have described the ACL as a continuum of numerous bundles (Arnoczky, 1983; Odensten and Gillquist, 1985; Skelley et al., 2017). The data in the present study demonstrates that the inverse correlation between attachment site to attachment site ACL length and flexion angle holds for both the AM and PL subdivisions throughout treadmill gait. These findings are consistent with previous *in vivo* studies that have also shown that bundles of the ACL function in parallel, with both bundles being longer in extension during weight-bearing knee flexion (Jordan et al., 2007; Li et al., 2004; Utturkar et al., 2013), dynamic single legged jumping (Englander et al., 2019), and unloaded knee flexion (Yoo et al., 2010). These differences in the relationship of the bundle function may be due to differences in the loading conditions applied to the joint, as noted by previous investigators (Andersen and Amis, 1994; Li et al., 2005).

Abnormal gait kinematics can occur as a result of ACL injury (Andriacchi and Dyrby, 2005; Georgoulis et al., 2003), and may persist after reconstruction (Georgoulis et al., 2007; Tashman et al., 2007). Interestingly, altered tibial translation and rotation were measured in ACL deficient patients as the knee extended just prior to heel strike (Andriacchi and Dyrby, 2005), which is the same period of the gait cycle where we measured peaks in attachment site to attachment site ACL length and strain in the present study. Thus, the findings of the present study may help explain altered gait kinematics related to ACL deficiency. Furthermore, data describing how the native ACL functions during gait may inform

reconstruction techniques that reduce possible gait deficits in the injured knee (Abebe et al., 2011; Andriacchi and Dyrby, 2005; Berchuck et al., 1990; Gao and Zheng, 2010; Georgoulis et al., 2003; Tashman et al., 2007) and thus potentially reduce the risk of cartilage degeneration (Andriacchi and Mundermann, 2006; Andriacchi et al., 2004; DeFrate, 2017). Additionally, these data may be useful in the design of rehabilitation (Fleming et al., 2001; Heijne et al., 2004) and injury prevention protocols (Shin et al., 2011), as well as in the validation mathematical models of ACL function (Shelburne et al., 2004; Weinhandl et al., 2016).

It is important to note that in this study attachment site to attachment site ACL strain was approximated by normalizing attachment site to attachment site ACL length to a reference length measured in a non-weight bearing, extended position during MR imaging. However, in general it is difficult to know precisely the unloaded reference length of the ACL *in vivo* since it cannot support axial compression (Taylor et al., 2013). Although there remains uncertainty in the unloaded length of the ACL, which may affect the magnitudes of strain (Fleming et al., 1994), peaks in the estimated and true strains should still occur concurrently. To this point, we observed similar timing of the peaks of attachment site to attachment site ACL strain as another *in vivo* study that measured ACL strain during gait from our laboratory, which used quiet standing as the reference position for strain calculations (Taylor et al., 2013). Furthermore, despite reported differences in over-ground versus treadmill gait (Alton et al., 1998; Parvataneni et al., 2009), we found a similar timing of peaks in ACL strain and similar relationships between flexion angle and attachment site to attachment site ACL length as reported previously by our laboratory (Taylor et al. 2013). Another important consideration is that these measurements are geometric in nature and do not directly measure tissue load. However, the techniques used in this study are advantageous in that they allow for a non-invasive *in vivo* estimation of attachment site to attachment site ACL length and strain under physiologic loading conditions. These measurements may be used in the future to help inform boundary conditions in computational modeling studies of ACL function (Limbirt et al., 2004; Mesfar and Shirazi-Adl, 2005).

In summary, 3D models of the knee joint derived from MR images were registered to high-speed biplanar radiographs to reproduce the *in vivo* positions of the bones and associated ACL attachment sites. Additionally, the attachment site to attachment site lengths of the ACL and its AM and PL bundles were measured throughout a full cycle of treadmill gait. Our main findings were that local maxima in attachment site to attachment site lengths of the ACL and its bundles were observed at heel strike and during midstance when the knee was extended. Furthermore, we demonstrated that the attachment site to attachment site lengths of the ACL and its bundles were inversely correlated with knee flexion throughout the gait cycle. This study provides valuable information on the function of the ACL and its bundles during treadmill gait.

Acknowledgements

This work was supported by NIH grants AR065527, AR075399, and AR074800. The authors gratefully acknowledge Dr. Robert E. Reiman for providing guidance on radiation safety as well as the assessment of radiation exposure and dosage. The authors gratefully acknowledge Edward L. Baldwin III and Wyatt A.R. Smith for their technical assistance.

Declaration of Competing Interest

The authors of this manuscript have no conflicts of interest pertaining to this work to disclose.

References

- Abebe, E.S., Moorman, C., Dziedzic, T.S., Spritzer, C.E., Cothran, R.L., Taylor, D.C., Garrett, W.E., DeFrate, L.E., 2009. Femoral tunnel placement during anterior cruciate ligament reconstruction *in vivo* imaging analysis comparing transtibial and 2-incision tibial tunnel-independent techniques. *Am. J. Sports Med.*, 37, 1904–1911.
- Abebe, E.S., Utturkar, G., Taylor, D., Spritzer, C., Kim, J., Moorman III, C., Garrett, W., DeFrate, L., 2011. The effects of femoral graft placement on *in vivo* knee kinematics after anterior cruciate ligament reconstruction. *J. Biomech.* 44, 924–929.
- Alton, F., Baldey, L., Caplan, S., Morrissey, M., 1998. A kinematic comparison of overground and treadmill walking. *Clin. Biomech.* 13, 434–440.
- Amis, A., Dawkins, G., 1991. Functional anatomy of the anterior cruciate ligament. Fibre bundle actions related to ligament replacements and injuries. *J. Bone Joint Surg. Brit.* 73, 260–267.
- Andersen, H.N., Amis, A.A., 1994. Review on tension in the natural and reconstructed anterior cruciate ligament. *Knee Surg. Sports Traumatol. Arthrosc.* 2, 192–202.
- Andriacchi, T.P., Dyrby, C.O., 2005. Interactions between kinematics and loading during walking for the normal and ACL deficient knee. *J. Biomech.* 38, 293–298.
- Andriacchi, T.P., Mundermann, A., 2006. The role of ambulatory mechanics in the initiation and progression of knee osteoarthritis. *Curr. Opin. Rheumatol.* 18, 514–518.
- Andriacchi, T.P., Mundermann, A., Smith, R.L., Alexander, E.J., Dyrby, C.O., Koo, S., 2004. A framework for the *in vivo* pathomechanics of osteoarthritis at the knee. *Ann. Biomed. Eng.* 32, 447–457.
- Arms, S.W., Pope, M.H., Johnson, R.J., Fischer, R.A., Arvidsson, I., Eriksson, E., 1984. The biomechanics of anterior cruciate ligament rehabilitation and reconstruction. *Am. J. Sports Med.* 12, 8–18.
- Arnoczky, S.P., 1983. Anatomy of the anterior cruciate ligament. *Clin. Orthopaed. Related Res.*, 19–25.
- Berchuck, M., Andriacchi, T., Bach, B., Reider, B., 1990. Gait adaptations by patients who have a deficient anterior cruciate ligament. *J. Bone Joint Surg.*, 871–877.
- Berns, G.S., Hull, M., Patterson, H.A., 1992. Strain in the anteromedial bundle of the anterior cruciate ligament under combination loading. *J. Orthopaed. Res.* 10, 167–176.
- Beynon, B.D., Fleming, B.C., 1998. Anterior cruciate ligament strain *in vivo*: a review of previous work. *J. Biomech.* 31, 519–525.
- Budd, H., Patchava, A., Khanduja, V., 2012. Establishing the radiation risk from fluoroscopic-assisted arthroscopic surgery of the hip. *Int. Orthopaed.* 36, 1803–1806.
- Butler, D.L., Noyes, F., Grood, E., 1980. Ligamentous restraints to anterior-posterior drawer in the human knee. A biomechanical study. *JBJS* 62, 259–270.
- Cerulli, G., Benoit, D., Lamontagne, M., Caraffa, A., Liti, A., 2003. *In vivo* anterior cruciate ligament strain behaviour during a rapid deceleration movement: case report. *Knee Surg. Sports Traumatol. Arthrosc.* 11, 307–311.
- Collins, A.T., Kulvaranon, M.L., Cutcliffe, H.C., Utturkar, G.M., Smith, W.A., Spritzer, C. E., Guilak, F., DeFrate, L.E., 2018. Obesity alters the *in vivo* mechanical response and biochemical properties of cartilage as measured by MRI. *Arth. Res. Ther.* 20, 232.
- DeFrate, L.E., 2017. Effects of ACL graft placement on *in vivo* knee function and cartilage thickness distributions. *J. Orthopaed. Res.* 35, 1160–1170.
- DeFrate, L.E., Nha, K.W., Papannagar, R., Moses, J.M., Gill, T.J., Li, G., 2007. The biomechanical function of the patellar tendon during *in vivo* weight-bearing flexion. *J. Biomech.* 40, 1716–1722.
- DeMorat, G., Weinhold, P., Blackburn, T., Chudik, S., Garrett, W., 2004. Aggressive quadriceps loading can induce noncontact anterior cruciate ligament injury. *Am. J. Sports Med.* 32, 477–483.
- Draganich, L., Vahey, J., 1990. An *in vitro* study of anterior cruciate ligament strain induced by quadriceps and hamstrings forces. *J. Orthopaed. Res.* 8, 57–63.
- Dürselen, L., Claes, L., Kiefer, H., 1995. The influence of muscle forces and external loads on cruciate ligament strain. *Am. J. Sports Med.* 23, 129–136.
- Englander, Z.A., Baldwin, E.L., Smith, W.A.R., Garrett, W.E., Spritzer, C.E., DeFrate, L. E., 2019a. *In vivo* anterior cruciate ligament deformation during a single-legged jump measured by magnetic resonance imaging and high-speed biplanar radiography. *Am. J. Sports Med.* In press.
- Englander, Z.A., Cutcliffe, H.C., Utturkar, G.M., Garrett, W.E., Spritzer, C.E., DeFrate, L. E., 2019. A comparison of knee abduction angles measured by a 3D anatomic coordinate system versus videographic analysis: implications for anterior cruciate ligament injury. *Orthopaed. J. Sports Med.* 7. In press.
- Englander, Z.A., Cutcliffe, H.C., Utturkar, G.M., Taylor, K.A., Spritzer, C.E., Garrett, W. E., DeFrate, L.E., 2019c. *In vivo* assessment of the interaction of patellar tendon tibial shaft angle and anterior cruciate ligament elongation during flexion. *J. Biomech.* 90, 123–127.
- Englander, Z.A., Martin, J.T., Ganapathy, P.K., Garrett, W.E., DeFrate, L.E., 2018. Automatic registration of MRI-based joint models to high-speed biplanar radiographs for precise quantification of *in vivo* anterior cruciate ligament deformation during gait. *J. Biomech.* 81, 36–44.
- Fleming, B.C., Beynon, B.D., 2004. *In vivo* measurement of ligament/tendon strains and forces: a review. *Ann. Biomed. Eng.* 32, 318–328.
- Fleming, B.C., Beynon, B.D., Tohyama, H., Johnson, R.J., Nichols, C.E., Renström, P., Pope, M.H., 1994. Determination of a zero strain reference for the anteromedial band of the anterior cruciate ligament. *J. Orthopaed. Res.* 12, 789–795.
- Fleming, B.C., Renstrom, P.A., Beynon, B.D., Engstrom, B., Peura, G.D., Badger, G.J., Johnson, R.J., 2001. The effect of weightbearing and external loading on anterior cruciate ligament strain. *J. Biomech.* 34, 163–170.

- Gabriel, M.T., Wong, E.K., Woo, S.L.-Y., Yagi, M., Debski, R.E., 2004. Distribution of in situ forces in the anterior cruciate ligament in response to rotatory loads. *J. Orthopaed. Res.* 22, 85–89.
- Gao, B., Zheng, N.N., 2010. Alterations in three-dimensional joint kinematics of anterior cruciate ligament-deficient and-reconstructed knees during walking. *Clin. Biomech.* 25, 222–229.
- Georgoulis, A.D., Papadonikolakis, A., Papageorgiou, C.D., Mitsou, A., Stergiou, N., 2003. Three-dimensional tibiofemoral kinematics of the anterior cruciate ligament-deficient and reconstructed knee during walking. *Am. J. Sports Med.* 31, 75–79.
- Georgoulis, A.D., Ristanis, S., Chouliaras, V., Moraiti, C., Stergiou, N., 2007. Tibial rotation is not restored after ACL reconstruction with a hamstring graft. *Clin. Orthopaed. Relat. Res.* 454, 89–94.
- Girgis, F.G., Marshall, J.L., Monajem, A., 1975. The cruciate ligaments of the knee joint. Anatomical, functional and experimental analysis. *Clin. Orthopaed. Relat. Res.* 216–231.
- Hara, K., Mochizuki, T., Sekiya, I., Yamaguchi, K., Akita, K., Muneta, T., 2009. Anatomy of normal human anterior cruciate ligament attachments evaluated by divided small bundles. *Am. J. Sports Med.* 37, 2386–2391.
- Hefzy, M., Grood, E., 1986. Sensitivity of insertion locations on length patterns of anterior cruciate ligament fibers. *J. Biomech. Eng.* 108, 73–82.
- Heijne, A., Fleming, B.C., Renstrom, P.A., Peura, G.D., Beynon, B.D., Werner, S., 2004. Strain on the anterior cruciate ligament during closed kinetic chain exercises. *Med. Sci. Sports Exerc.* 36, 935–941.
- Huber, C., Nüesch, C., Göpfert, B., Cattin, P.C., von Tscharnner, V., 2011. Muscular timing and inter-muscular coordination in healthy females while walking. *J. Neurosci. Methods* 201, 27–34.
- Jordan, S.S., DeFrate, L.E., Wook Nha, K., Papannagari, R., Gill, T.J., Li, G., 2007. The in vivo kinematics of the anteromedial and posterolateral bundles of the anterior cruciate ligament during weightbearing knee flexion. *Am. J. Sports Med.* 35, 547–554.
- Kim, S.Y., Spritzer, C.E., Utturkar, G.M., Toth, A.P., Garrett, W.E., DeFrate, L.E., 2015. Knee kinematics during noncontact anterior cruciate ligament injury as determined from bone bruise location. *Am. J. Sports Med.* 43, 2515–2521.
- Li, G., DeFrate, L.E., Rubash, H.E., Gill, T.J., 2005. In vivo kinematics of the ACL during weight-bearing knee flexion. *J. Orthopaed. Res.* 23, 340–344.
- Li, G., DeFrate, L.E., Sun, H., Gill, T.J., 2004. In vivo elongation of the anterior cruciate ligament and posterior cruciate ligament during knee flexion. *Am. J. Sports Med.* 32, 1415–1420.
- Limbirt, G., Taylor, M., Middleton, J., 2004. Three-dimensional finite element modelling of the human ACL: simulation of passive knee flexion with a stressed and stress-free ACL. *J. Biomech.* 37, 1723–1731.
- Markolf, K.L., Gorek, J.F., Kabo, J.M., Shapiro, M.S., 1990. Direct measurement of resultant forces in the anterior cruciate ligament. An in vitro study performed with a new experimental technique. *JBJS* 72, 557–567.
- Marouane, H., Shirazi-Adl, A., Adouni, M., Hashemi, J., 2014. Steeper posterior tibial slope markedly increases ACL force in both active gait and passive knee joint under compression. *J. Biomech.* 47, 1353–1359.
- Marouane, H., Shirazi-Adl, A., Hashemi, J., 2015. Quantification of the role of tibial posterior slope in knee joint mechanics and ACL force in simulated gait. *J. Biomech.* 48, 1899–1905.
- Mesfar, W., Shirazi-Adl, A., 2005. Biomechanics of the knee joint in flexion under various quadriceps forces. *Knee* 12, 424–434.
- Mettler Jr, F.A., Bhargavan, M., Faulkner, K., Gilley, D.B., Gray, J.E., Ibbott, G.S., Lipoti, J.A., Mahesh, M., McCrohan, J.L., Stabin, M.G., 2009. Radiologic and nuclear medicine studies in the United States and worldwide: frequency, radiation dose, and comparison with other radiation sources—1950–2007. *Radiology* 253, 520–531.
- Meyer, E.G., Haut, R.C., 2005. Excessive compression of the human tibio-femoral joint causes ACL rupture. *J. Biomech.* 38, 2311–2316.
- Meyer, E.G., Haut, R.C., 2008. Anterior cruciate ligament injury induced by internal tibial torsion or tibiofemoral compression. *J. Biomech.* 41, 3377–3383.
- Nawabi, D.H., Tucker, S., Schafer, K.A., Zuiderbaan, H.A., Nguyen, J.T., Wickiewicz, T. L., Imhauser, C.W., Pearle, A.D., 2016. ACL fibers near the lateral intercondylar ridge are the most load bearing during stability examinations and isometric through passive flexion. *Am. J. Sports Med.* 44, 2563–2571.
- NCRP, 2010. Radiation Dose Management for Fluoroscopically Guided Interventional Medical Procedures, NCRP Report No. 168. National Council on Radiation Protection and Measurements (NCRP), Bethesda, Maryland.
- Norwood Jr, L.A., Cross, M.J., 1977. The intercondylar shelf and the anterior cruciate ligament. *Am. J. Sports Med.* 5, 171–176.
- Nunley, R.M., Wright, D., Renner, J.B., Yu, B., Garrett Jr, W.E., 2003. Gender comparison of patellar tendon tibial shaft angle with weight bearing. *Res. Sports Med.* 11, 173–185.
- Odensten, M., Gillquist, J., 1985. Functional anatomy of the anterior cruciate ligament and a rationale for reconstruction. *J. Bone Joint Surg. Am.* 67, 257–262.
- Otsubo, H., Shino, K., Suzuki, D., Kamiya, T., Suzuki, T., Watanabe, K., Fujimiyama, M., Iwahashi, T., Yamashita, T., 2012. The arrangement and the attachment areas of three ACL bundles. *Knee Surg. Sports Traumatol. Arthrosc.* 20, 127–134.
- Owusu-Akyaw, K.A., Kim, S.Y., Spritzer, C.E., Collins, A.T., Englander, Z.A., Utturkar, G.M., Garrett, W.E., DeFrate, L.E., 2018. Determination of the position of the knee at the time of an anterior cruciate ligament rupture for male versus female patients by an analysis of bone bruises. *Am. J. Sports Med.* 46, 1559–1565.
- Parvataneni, K., Ploeg, L., Olney, S.J., Brouwer, B., 2009. Kinematic, kinetic and metabolic parameters of treadmill versus overground walking in healthy older adults. *Clin. Biomech.* 24, 95–100.
- Petersen, W., Zantop, T., 2007. Anatomy of the anterior cruciate ligament with regard to its two bundles. *Clinical Orthopaedics and Related Research* 454, 35–47.
- Reimann, D.A., Flynn, M.J., 1992. Year Automated distortion correction of x-ray image intensifier images. Nuclear Science Symposium and Medical Imaging Conference, Conference Record of the 1992 IEEE.
- Shelburne, K.B., Pandey, M.G., Anderson, F.C., Torry, M.R., 2004. Pattern of anterior cruciate ligament force in normal walking. *J. Biomech.* 37, 797–805.
- Shin, C.S., Chaudhari, A.M., Andriacchi, T.P., 2011. Valgus plus internal rotation moments increase anterior cruciate ligament strain more than either alone. *Med. Sci. Sports Exerc.* 43, 1484–1491.
- Skellej, N.W., Lake, S.P., Brophy, R.H., 2017. Microstructural properties of the anterior cruciate ligament. *Annals of Joint* 2.
- Tashman, S., Kolowich, P., Collon, D., Anderson, K., Anderst, W., 2007. Dynamic function of the ACL-reconstructed knee during running. *Clin. Orthopaed. Relat. Res.* 454, 66–73.
- Taylor, K., Cutcliffe, H., Queen, R., Utturkar, G., Spritzer, C., Garrett, W., DeFrate, L., 2013. In vivo measurement of ACL length and relative strain during walking. *J. Biomech.* 46, 478–483.
- Taylor, K., Terry, M., Utturkar, G., Spritzer, C., Queen, R., Iribarra, L., Garrett, W., DeFrate, L., 2011. Measurement of in vivo anterior cruciate ligament strain during dynamic jump landing. *J. Biomech.* 44, 365–371.
- Torzilli, P.A., Deng, X., Warren, R.F., 1994. The effect of joint-compressive load and quadriceps muscle force on knee motion in the intact and anterior cruciate ligament-sectioned knee. *Am. J. Sports Med.* 22, 105–112.
- Utturkar, G., Iribarra, L., Taylor, K., Spritzer, C., Taylor, D., Garrett, W., DeFrate, L.E., 2013. The effects of a valgus collapse knee position on in vivo ACL elongation. *Ann. Biomed. Eng.* 41, 123–130.
- Weinhandl, J.T., Hoch, M.C., Bawab, S.Y., Ringleb, S.I., 2016. Comparison of ACL strain estimated via a data-driven model with in vitro measurements. *Comput. Methods Biomech. Biomed. Eng.* 19, 1550–1556.
- Wu, J.L., Hosseini, A., Kozanek, M., Gadikota, H.R., Gill IV, T.J., Li, G., 2010. Kinematics of the anterior cruciate ligament during gait. *Am. J. Sports Med.* 38, 1475–1482.
- Yoo, Y.-S., Jeong, W.-S., Shetty, N.S., Ingham, S.J.M., Smolinski, P., Fu, F., 2010. Changes in ACL length at different knee flexion angles: an in vivo biomechanical study. *Knee Surg. Sports Traumatol. Arthrosc.* 18, 292–297.